

Infrared retrievals of dust using AIRS: Comparisons of optical depths and heights derived for a North African dust storm to other collocated EOS A-Train and surface observations

S. G. DeSouza-Machado,¹ L. L. Strow,¹ B. Imbiriba,¹ K. McCann,¹ R. M. Hoff,¹ S. E. Hannon,¹ J. V. Martins,¹ D. Tanré,² J. L. Deuzé,² F. Ducos,² and O. Torres³

Received 17 July 2009; revised 16 February 2010; accepted 6 April 2010; published 3 August 2010.

[1] AIRS thermal infrared radiance data are used with a fast infrared scattering radiative transfer model to physically retrieve the dust column amount and dust height over both ocean and land. The retrieved optical depths are compared against those retrieved using visible and ultraviolet instruments on the A-Train, while dust layer heights are evaluated against lidar data. The synergistic use of AIRS data is explored by using dust layer heights constrained by CALIPSO retrievals and coarse mode particle sizes over ocean from PARASOL. Optical depths from AIRS correlate well with those from other instruments over ocean ($R \geq 0.9$) and are lower over land when compared to MODIS Deep Blue and OMI retrievals ($R \leq 0.8$). AIRS-derived dust top heights compare favorably with CALIPSO data and can be used to improve OMI optical depth retrievals over a much larger area than CALIPSO can provide. AIRS data can also provide estimates of dust longwave radiative forcing. For the examples examined here, the forcings are estimated to be about +1.5 and +4.5 W/m² per unit visible optical depth over ocean and land, respectively, compared to a shortwave forcing estimate of −50 W/m² over ocean. AIRS dust retrievals are possible day or night, can provide dust column amount information over land or ocean, and are unaffected by areas of the oceans covered by sun glint.

Citation: DeSouza-Machado, S. G., et al. (2010), Infrared retrievals of dust using AIRS: Comparisons of optical depths and heights derived for a North African dust storm to other collocated EOS A-Train and surface observations, *J. Geophys. Res.*, 115, D15201, doi:10.1029/2009JD012842.

1. Introduction

[2] Aerosols play an important, yet not completely understood, role in climate change and global warming. The uncertainty in aerosol direct radiative forcing is about 40% greater than that from greenhouse gases, while the total uncertainty in radiative forcing due to the direct and indirect aerosol effects is a significant fraction of the total anthropogenic radiative forcing [*Intergovernmental Panel on Climate Change (IPCC)*, 2007]. Mineral desert dust is spatially and temporally variable, making it difficult to study its effect on radiative forcing. Dust storms spread over vast geographical areas and are now more frequent, partly due to climatic variability and land use change such as deforestation or overgrazing [*Jickells et al.*, 2005]. Radiative forcing

due to dust storms can affect atmospheric processes on various spatial and temporal scales [*Lubin et al.*, 2002; *Sokolik*, 2002; *Gu et al.*, 2003], leading to, for example, drying of dust laden atmospheric layers. The transported dust can also affect local ecosystems by killing coral [*Jickells et al.*, 2005], fertilizing ocean phytoplankton [*Kaufman et al.*, 2005] and transporting mineral nutrients from the Bodele region in Central Africa all the way to the Amazon Forest [*Koren et al.*, 2006].

[3] Space based remote sensing instruments are capable of detecting dust storms with nearly daily global coverage. Significant contributions have already been made from visible (VIS) and ultraviolet (UV) instruments. However, several papers point out that little research exists on the radiative effects of dust in the longwave or thermal infrared (TIR) [*Lubin et al.*, 2002; *Yu et al.*, 2006; *Shell and Somerville*, 2007]. These include the impact of surface and top-of-atmosphere longwave forcing by dust on weather and climate [*Shell and Somerville*, 2007]. Examination of atmospheric parameters retrieved from dust contaminated Fields of View (FOVs) from thermal sounding instruments shows that dust negatively impacts the retrievals, degrading

¹Physics Department and Joint Center for Earth Systems Technology, University of Maryland Baltimore County, Baltimore, Maryland, USA.

²Atmospheric Laboratory of Optics, University of Sciences and Technologies of Lille, Lille, France.

³Department of Atmospheric and Planetary Sciences, Hampton University, Hampton, Virginia, USA.

Table 1. AIRS Dust Flag Detection Over Ocean^a

Classification	Test Channel BTD ^b	Score
dust0	$\text{find}((b-d) \geq -0.5 \text{ and } (b-d) \leq 1.00)$	1
dust1	$\text{find}((d-e) \leq -1.25)$	2
dust2	$\text{find}((d-a) \leq -0.75)$	4
dust3	$\text{find}((c-d) \geq -0.2 \text{ and } (c-d) \leq 1.0)$	8
dust4	$\text{find}((b-e) \geq -4.5 \text{ and } (b-e) \leq -0.3)$	16
dust5	$\text{find}((b-a) \leq 0.115)$	32
dust6	$\text{find}((b-c) \geq 0.05 \text{ and } (b-c) \leq 1.5)$	64
dust7	$\text{find}((c-a) \leq 0.40)$	128
dust8	$\text{find}((c-e) \leq -0.15)$	256

^aOcean threshold = 380.^bChannel centers (a)–(e) are 822.4, 900.3, 961.1, 1129.0 and 1231.3 cm^{-1} respectively. Thresholds for tests 7 and 8 must be modified for best performance over land. BTD denotes brightness temperature differences.

the use of the data in weather forecasting over vast regions [De Souza-Machado et al., 2006].

[4] TIR instruments are capable of detecting mineral dust day and night, and are also sensitive to the vertical placement of the dust layer. Dust affects the scattered UV radiances, determines the stability of the atmosphere, can either warm or cool the atmospheric column (depending on the albedo of the underlying surface), and has an indirect effect on rain-producing clouds [Joseph et al., 2008]. Desert dust is one of the principal contributors to the atmosphere's aerosol burden. An improved determination of the dust layer height will help understand the dust life cycle and better estimate the long wave forcing due to dust [IPCC, 2007].

[5] This paper focuses on a late February 2007 dust storm generated by a mid latitude weather system arriving over northwest Africa and then advecting over northern Sahara into the Eastern Mediterranean. TIR hyperspectral sounding data from the Atmospheric Infra-Red Sounder (AIRS) is used to study the dust storm over ocean and land. Sounding data from this instrument is used primarily for weather forecasting and climate studies, but also contains information about dust optical depths τ and dust layer heights. Where possible we use a fusion of data from other instruments on the “A-train” missions, such as dust coarse mode effective particle radii derived over ocean from POLDER (POLarization and Directionality of the Earth's Reflectances). Dust layer heights are compared against the extinction backscatter profiles obtained from the CALIOP (Cloud-Aerosol Lidar with Orthogonal Polarization) lidar. TIR optical depths are evaluated against those from three other A-Train VIS/UV instruments: POLDER, Moderate Resolution Imaging Spectroradiometer (MODIS), and Ozone Monitoring Instrument (OMI) on the PARASOL, Aqua, and Aura platforms respectively, as well as against those obtained from the integrated column CALIOP data. Where possible, comparisons are made against retrievals reported from AERONET observation sites [Holben et al., 1998]. Daytime examples are mainly shown for comparison purposes with MODIS, OMI and PARASOL since they require reflected solar radiation for dust retrievals. Finally we use AIRS radiances to estimate the Outgoing Longwave Radiation (OLR) forcing due to dust over ocean, and compare against estimates obtained using MODIS data.

[6] The NASA's AIRS L2 operational retrieval system currently only produces a dust detection flag. The work

reported here is a candidate algorithm for future AIRS processing, and could be used to improve operational AIRS L2 retrievals under dust conditions. It should also help address the uncertainties in longwave forcing due to dust.

[7] Section 3 outlines the retrieval algorithm for the AIRS instrument, while Section 4 discusses the other A-Train instruments used in this study. An in-depth description of the dust storm analyzed here is then presented. Section 5 describes the meteorological conditions associated with this dust storm, using European Center for Medium-Range Weather Forecasts (ECMWF) analysis 3 hour forecast model data, surface observations and VIS/IR data. Sections 6 and 7 present an analysis of heights and optical depths retrieved by the A-Train instruments. Estimates of the OLR forcing associated with the dust storm are presented in Section 8, followed by conclusions in Section 9.

2. Detecting FOVS Containing Dust

[8] The AIRS v4+ processing system flags dust contaminated FOVs in the Level 1B (L1B) geolocated radiance data sets. A dust-detection algorithm (DDA) computes brightness temperature differences (BTDs) for five AIRS channels in the 10 μm atmospheric window region. These BTDs undergo a number of tests to generate a summed score, with the FOV tagged “dusty” if the scores exceeds a threshold of 380 over ocean. Table 1 summarizes this algorithm. Comparisons against visible images and retrieved MODIS aerosol optical depths show the flag produces very few false positives when used over tropical and mid-latitude oceans. The wave numbers of the channels used in the DDA are listed in Table 1, and are shown in Figure 1. These channels

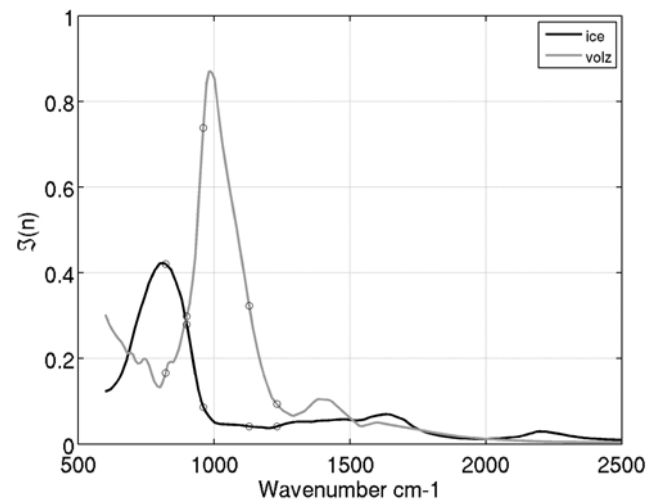


Figure 1. Imaginary part (absorptive component) of ice and dust refractive indices. The Volz Saharan dust data is used for this plot. The circles show the locations of the AIRS channels used for the dust flag. Note that dust has a peak absorption at about 10 μm (1000 cm^{-1}) while ice has a peak absorption at longer wavelengths (about 12 μm or 800 cm^{-1}). This spectral separation can allow IR instruments to discriminate between the presence of ice or dust in a FOV. Ozone also has peak absorption in the 1000–1080 cm^{-1} region.

were chosen since they have low noise, span either side of the region of strong IR dust absorption, and avoid water lines. The region of peak dust absorption between 1000–1100 cm^{-1} is not used, as it coincides with the region of peak ozone absorption in the IR.

[9] The DDA tests shown in Table 1 assume an underlying ocean emissivity. Altering the *dust7*, *dust8* thresholds and lowering the cumulative threshold to 360 yields moderately successful dust detection over the Sahara. Further improvement would require a lookup table of thresholds that varies temporally and spatially with surface emissivity. The current settings over land were qualitatively verified using visual comparisons with Aqua-MODIS images and those from the Spinning Enhanced Visible and Infrared Imager (SEVIRI) on board Meteosat Second Generation. SEVIRI is a geostationary instrument positioned above Europe and Africa acquiring $\simeq 1$ km (VIS) and 3 km (IR) data every 15 minutes. SEVIRI daily false color maps showing dust detection using the EUMETSAT algorithm can be seen at http://loaamma.univ-lille1.fr/AMMA/MET/gall_2007.php.

[10] The DDA test has several limitations. Different combinations of dust layer heights and optical depths can produce very similar radiances. Thus the simple DDA test will not provide quantitative information on either of these variables. Nonetheless, it is still useful to estimate minimum detectable dust optical depths. If one assumes a tropical ocean scene, with low lying dust at a height of 1.5 km, the AIRS channels' noise levels suggest the DDA will detect dust with visible optical depths of greater than $\simeq 0.2$, with increasing sensitivity as the dust layer rises. The DDA is a simple method for automating a search for dust in the AIRS radiances, and is implemented in the AIRS L2 retrieval algorithm. The main purpose of the DDA is to quickly determine if the dust content of a scene is large enough to warrant a more sophisticated retrieval. This is of great practical importance since the vast majority of scenes will not contain dust. The DDA plays a relatively minor role in this study, as it is used to select which FOVs we feed into the dust optical depth retrieval algorithm. The ultimate limits of dust detection with the DDA algorithm have not been explored.

3. AIRS Dust Retrieval Algorithm

[11] AIRS has 2378 channels covering 649–1136, 1217–1613, 2181–2665 cm^{-1} (8.8–15.4, 6.2–8.2, 3.75–4.58 μm). The full widths at half maximum satisfy $\nu/\delta\nu \simeq 1200$, with the noise equivalent change in temperature ($NE\Delta T$) $\simeq 0.2$ K. Each cross track swath consists of 90 FOVs, with a 15 km nadir footprint.

[12] The almost complete high-resolution spectral coverage of the 8–12 μm atmospheric window has been used to detect silicate based aerosols [Pierangelo *et al.*, 2005; De Souza-Machado *et al.*, 2006]. The 10 μm TIR window channels are most sensitive to the height and optical depth of the dust layer, and less sensitive to modal particle size or size distribution. The 4 μm window channels on AIRS are more sensitive to optical depth. Together, AIRS data from these two regions allow for retrieval of dust height and loading, day and night over ocean and land, even under sun glint conditions.

[13] The transfer of infrared radiation in a scattering, absorbing and emitting atmosphere is computed using the algorithm by Chou *et al.* [1999]. In this scheme, the scattering by the dust is approximated through the use of a scaled optical depth to account for radiation scattered upwards and downward. The AIRS Radiative Transfer Algorithm (AIRS-RTA) models the atmosphere using 100 pressure layers, with a lower tropospheric layer thickness of $\simeq 0.25$ km. Dust is placed within one vertical “slab” defined by two bounding pressures, which spans a few consecutive AIRS-RTA layers. The dust is distributed among these layers in proportion to the change in pressure across the layer divided by the total change in pressure across the slab. This approximates a constant dust mass mixing ratio over these layers.

[14] This work uses a physical retrieval algorithm to derive the dust optical depth and height, while a lookup table approach is used by Pierangelo *et al.* [2004]. A statistically accurate estimate of the atmospheric state from ECMWF and/or direct surface observations initializes the retrieval, which is stabilized by constraining the effective particle size, and dust top height along with the dust layer thickness. After linearizing the radiative transfer equation about a starting guess, a Newton-Raphson (NR) method fits for the column dust loading Γ (in g/m^2) by minimizing the differences between observations and calculations. 25 channels spanning the 780–980 cm^{-1} range, seven channels spanning 1080–1130 cm^{-1} , and four channels located at 1228, 1231, 2602, and 2616 cm^{-1} are equally weighted in this minimization procedure. In the 4 μm region, the radiance for daytime scenes includes the solution from Chou *et al.* [1999], and the effects of solar beam scattering plus the downwelling solar contribution reflected by the surface. We recognize the radiances in these 4 μm channels are sensitive to the details of the phase function, which in our code is approximated using the Henyey-Greenstein phase function. On the second iteration small errors in the RTA scattering are mostly accounted for by least-squares adjustments to the surface reflectivity, if needed.

[15] A first guess for the dust loading Γ (g/m^2) is made using the 4 and 10 μm window channels. The 1228 and 1231 cm^{-1} channels are then used to adjust the surface temperature, as they are only weakly affected by dust and water; this is followed by an adjustment to the dust amount. Finally a second surface temperature adjustment is made, followed by a third and final dust amount estimate. In this paper, infrared optical depths are reported at 900 cm^{-1} (11.1 μm), well away from the peak ozone absorption. The retrieved dust loading is related to the reported TIR dust optical depth τ_{IR} by

$$\tau_{\text{IR}}(\nu) = \sigma_{\text{dustmodel}}(\nu, r_{\text{mode}}) \times \Gamma \quad (1)$$

Here $\sigma_{\text{dustmodel}}(\nu, r_{\text{mode}})$ is the mass extinction efficiency in $\text{m}^2 \text{g}^{-1}$. The required 2–3 iterations take ≤ 0.1 seconds per FOV on a 2 GHz processor, rapid enough for an operational retrieval on FOVs tagged as dusty. For most dusty FOVs, the optical depths change by less than 10% between the second and third iterations.

[16] Ocean emissivities are from Masuda *et al.* [1988], while over land an emissivity database derived using the MODIS TIR channels is used, as described by Borbas *et al.*

[2007] is used. MODIS TIR channels are spectrally wider than AIRS (about 20–40 cm^{-1} compared to $\leq 1 \text{ cm}^{-1}$) with only about 10 channels spanning the 750–1300 cm^{-1} range. However, any database spectral limitations should be offset by averaging over many AIRS window channels.

3.1. AIRS Dust Height Retrieval Algorithm

[17] Correct placement of the dust layer is extremely important for dust optical depth retrievals from TIR and UV instruments. Climatological dust heights could be used, such as those from the Goddard Chemistry Aerosol Radiation and Transport (GOCART) model [Ginoux *et al.*, 2001] (as opposed to the model predictions for a given day). Dust height placement can also be taken directly from CALIOP, a nadir view lidar instrument on the A-Train, but it has very limited spatial coverage.

[18] The following dust height retrieval approach using AIRS data works well for the optically thick dust storms examined in this work, but could fail for tenuous or low altitude dust. For each FOV, dust is initially placed within the boundaries of one of the AIRS RTA pressure layers. These pressure layers are equivalent to those in the AIRS support product. A dust optical depth is retrieved, and the corresponding spectral residual is also saved. This process is repeated for each of the ≈ 20 pressure layers lying between 1–6 km above sea level. The top boundary of the layer that produces the smallest spectral residual is deemed the dust height for that FOV. Thus, in this paper, the term “dust height” always means the top layer boundary of the dust placed in our radiative transfer algorithm. In addition, this approach implies that we retrieve no information on the dust vertical extent. The results are then averaged over $0.5^\circ \times 0.5^\circ$ latitude-longitude grid boxes to estimate the mean and standard deviation of the dust top height. Over the tropical regions, this grid box corresponds to a 3×3 AIRS Field of Regard ($\approx 45 \text{ km}$), which is the horizontal resolution of the AIRS L2 products. Averaging over a smaller or larger grid box produces height fields with too much/too little variation, as seen from comparisons to available CALIOP data. A final dust optical depth retrieval for each FOV is then done using this gridded dust top height.

3.2. Sources of Error in TIR Optical Depth Retrievals

[19] Thermal infrared optical depth retrievals are sensitive to the atmospheric state A , dust optical constants, dust height (h) and particle sizes r_{eff} . Infrared retrievals are unstable unless constrained, as fitting for the observed radiance $r_{\text{obs}}(\nu, \theta)$ yields multiple non-unique solutions for $(A, \tau, h, r_{\text{eff}})$. Uncertainties in the constraints alter the retrieved optical depths as discussed below.

[20] Dust resides mainly in the troposphere where the negative lapse rate makes TIR retrievals of dust optical depths very sensitive to the dust height. A typical dust profile displaced upward by 1 km nearly halves the retrieved optical depth [De Souza-Machado *et al.*, 2006]. The retrieval uses atmospheric states initialized from the nearest 0.25° grid point in the ECMWF data fields. Well characterized sea surface emissivities, coupled with numerous weather observation stations in the Western Europe/Mediterranean region [Reale and Dutton, 2007] leaves the dust height estimation as the largest error source in TIR optical depth

retrievals over the ocean. Fewer weather observation stations over the Sahara, and less well characterized (quartz) desert surface emissivity, means errors over land regions can arise from both incorrect dust placement as well as inaccurate surface and profile parameters.

[21] The AIRS-RTA models the radiance for any AIRS channel by summing two main contributions, atmospheric emission and surface emission. The surface term lacks vertical information, as this is simply the surface emission attenuated by the total absorption by the gases and dust in the atmospheric column. Infrared instruments are sensitive to the atmospheric vertical structure because of the second term. Atmospheric emission is a weighted sum of Planck radiances emitted at the atmospheric layer temperatures $T(z)$. The weighting is computed from layer to space transmittances, which depend on the sum of the gas and dust absorption in each layer. In the thermal infrared window region used in this paper, the layer gas optical depths are small (the primary contribution being the water continuum absorption close to the surface), and the weighting functions are largest close to the surface. Placing dust in any of the atmospheric layers significantly enhances the weighting function in this and adjoining layers. This alters the weighting function, both moving the peak away from the surface and making it much narrower. The layers near this peak then contribute most strongly to the radiance computed by the AIRS-RTA. The dust height retrieval is then an optimal placement of dust achieved by balancing the enhanced weighting of the spectral Planck radiance emitted at the temperatures of these layers with the spectral dependence of the combined gas and dust absorptions, to find the best match between the computed radiances with the observed radiances.

[22] Relatively minor errors are introduced in the retrieval by constraining the dust to reside in a few layers in the AIRS RTA. If the dust layer thickness is increased, the retrieval will return a larger dust optical depth. The CALIOP 532 nm lidar depolarization ratio shows that the dust layers were $\leq 1 \text{ km}$ thick for typical cases examined in this paper. For example, placing dust in a 500 m thick layer (with the top at 2.1 km), would retrieve optical depths that are 20% smaller than those retrieved if the dust layer were doubled (with the dust top at the same level).

[23] The dust retrieval can be unstable if the height, amount, and mean particle size are all varied simultaneously. Since the dust particle size varies far less than height and amount, a fixed particle size distribution was generally used here, based on Mie scattering tables computed from a unimodal log-normal particle size distribution ($\sigma = 2 \text{ }\mu\text{m}$) [Lubin *et al.*, 2002]. The dust optical constants are from Volz [1973], which have been used in a number of previous Saharan dust storm studies [Highwood *et al.*, 2003; De Souza-Machado *et al.*, 2006; Hansell *et al.*, 2008].

3.3. Quality Control

[24] The dust detection algorithm (DDA) will sometimes select dusty FOV that also contain optically thin clouds, especially cirrus. A dust retrieval performed on these scenes will yield unphysically large dust optical depths. The first quality control check rejects the FOV if $BT(820) \leq 273 \text{ K}$, a clear indication of cloud contamination. If the dust retrieval

returns $|(obs - calc)| > 2K$ for both the 820 and 960 cm^{-1} channels the retrieval is also discarded. These high bias values indicate model surface emissivity or large residual surface temperature errors.

4. Other A-Train Instruments Used in This Study

[25] Visible and UV instruments are sensitive to both fine and coarse mode dust, and some report both individual and total (fine+coarse) optical depths. Since the wavelengths of the thermal infrared are typically much larger than dust particle sizes, the AIRS IR radiances are sensitive mainly to large coarse mode particles and relatively insensitive to fine mode particles. However, unless the dust has been transported over extremely large distances, the coarse mode is also dominant for Visible and UV dust retrievals, thus AIRS optical depth retrievals can be compared against total optical depth retrievals from the other instruments. OMI reports the total optical depth. MODIS can separate out the fine and coarse modes. PARASOL reports only the fine mode optical depth over land, so use is made of the total (fine+coarse) optical depth retrieved over ocean only. The retrieved TIR optical depths are typically about 2–5 times smaller than those retrieved from the other instruments, as expected from Mie theory with an assumed lognormal particle size distribution.

[26] The CALIOP lidar on CALIPSO [Winker *et al.*, 2004] provides optical properties and altitude resolution of clouds and aerosols, including dust. CALIOP is a two-wavelength lidar that transmits and receives backscattered light at laser wavelengths of 532 nm and 1064 nm. CALIOP also has a polarization channel for the 532 nm wavelength. The CALIOP laser has a 25.25 Hz repetition rate with a 70 meter surface footprint. The data have 30 m vertical resolution from the surface to 8 km altitude, and 60 m resolution above, with minimum horizontal resolution of a single profile of 1/3 km. A typical horizontal averaging interval is 5 km (15 profiles) for aerosols and dust. CALIOP is a nadir-only instrument, covering far less of the globe than AIRS. It follows a similar ground track to AIRS, offset by 170 km from AIRS nadir. Depending on the location of the dust storm with respect to the lidar beam, CALIPSO data could be used to constrain dust heights for $\simeq(1/90)$ of the AIRS FOVS.

[27] Currently available CALIOP data includes Level 1B calibrated and geolocated attenuated backscatter values ($\beta_{attenuation}$ [$\text{km}^{-1} \text{sr}^{-1}$]) as a function of altitude at 532 and 1064 nm. In this paper, we used mainly the 532 nm data to retrieve profiles of extinction ($\sigma_{ext}(532 \text{ nm})$ [km^{-1}]) versus altitude by solving the elastic lidar equation assuming an extinction to backscatter ratio ($S_a(532 \text{ nm}) = 40 \text{sr}$ value recommended by Omar *et al.* [2003]) and similar to the 41 sr value used by Liu *et al.* [2009]. For low dust loading, the CALIOP extinction data can be used with a single scattering assumption to retrieve the optical depths ($\tau_{VIS} \leq 1$). There are known issues with the production CALIOP L2 extinction data below 1 km [Ganguly *et al.*, 2009; M. Vaughan, personal communication, 2009]. Our results are consistent with the CALIOP L2 data, computed independently by the CALIOP team. When computing correlations against other instruments, we additionally smoothed the averaged data over $\simeq 15$ km.

[28] Launched on board the PARASOL satellite in December 2004 as part of the A-Train, the POLDER instrument provides measurements of the spectral, directional and polarized characteristics of the solar radiation reflected by the Earth-Atmosphere system. The signal to noise ratio of POLDER is increased by averaging the individual 5×6.5 km footprints over a 3×3 pixel grid, giving an aerosol optical depth resolution of $15 \text{ km} \times 19.5 \text{ km}$. Separate retrieval algorithms are used over land [Deuze *et al.*, 2001] and over ocean [Herman *et al.*, 2005], based on comparisons between POLDER measurements and lookup tables built for a set of aerosol models (size distribution, refractive index, optical thickness). Over ocean, the inversion scheme mainly uses the normalized total and polarized radiances in the 865 nm channel, where the ocean color reflectance is zero, and in the 670 nm channel with a constant water reflectance of 0.001. The algorithm uses a bimodal aerosol model and is able to discriminate between small spherical, large spherical and large non-spherical particles. When a wide range of viewing geometries is available, the aerosol retrieved parameters are the fine and total aerosol optical depth, non-sphericity index, Angstrom coefficient, effective radius of small particles, and refractive index of small and large spherical particles. Over land, it uses only the polarized radiance measurements, which limits the retrieved information to fine mode optical depths. For this paper, the POLDER cloud screening has been relaxed and so there may be some residual clouds. This provides more retrieval area coverage for comparisons against the other A-Train instruments.

[29] MODIS is a high spatial resolution instrument (≤ 1 km) that acquires data in 36 spectral bands ranging from the visible to the TIR [Barnes *et al.*, 1998]. The MODIS Level 2 products assume spherical particles to retrieve primary products, from which a number of other parameters are derived and reported such as mean particle size, fine/coarse mode ratio and Angstrom coefficients [Remer *et al.*, 2005]. All six visible and near infrared channels are used to find the best fit between a combination of models in a look up table and the measured radiances. Once the aerosol model is derived, the optical depth is retrieved from the 865 nm channel since it has the smallest uncertainties from background particles and water-leaving radiances. Over ocean we compare our results to the Effective Optical Depth Average Ocean total (fine+coarse) mode retrieval results. Over bright desert surfaces, the MODIS Deep Blue retrieval algorithm [Hsu *et al.*, 2004] is fundamentally different from the ocean retrieval algorithm. Comparisons between the Deep Blue algorithm and AERONET sun photometers show agreement to within 20% for dust retrievals over (bright) land surfaces [Hsu *et al.*, 2004].

[30] OMI is a nadir viewing UV-VIS spectrometer (270–500 nm) on the Aura satellite, with a 13×24 km nadir footprint. In this work, we use the optical depths reported by the OMI near UV (388 nm) aerosol algorithm (OMAERUV), converted to 500 nm [Torres *et al.*, 2007]. Over cloud free areas, the OMAERUV algorithm can retrieve the optical depths and the aerosol single scattering albedo. The accuracy of this product depends on the validity of the assumptions used in the retrieval, such as aerosol layer height and aerosol type. OMI retrievals differentiate between uv-absorbing (dust and smoke) and non-absorbing aerosols. An estimate for the

Table 2. Instrument Characteristics Used in This Study

Instrument	Footprint (km)	Retrieval (km)	Swath (km)	Available Channels	Height for Reported Retrieval
AIRS	15	15	2000	IR	900 cm ⁻¹ (11 μm)
CALIPSO	0.1	15	0	532, 1064 nm	532 nm
MODIS (land)	1	10	2330	Vis, NIR, IR	550 nm
MODIS (ocean)	1	10	2330	Vis, NIR, IR	858 nm
PARASOL	7 × 6	20	1600	UV, Vis, NIR	865 nm
OMI	13 × 24	13 × 24	2600	UV	500 nm
AERONET	point	point	ground	VIS	500 nm

height of the aerosol layer is needed for smoke and dust. For dust the aerosol layer height is taken from a GOCART generated global climatology of aerosol vertical distribution.

[31] For ease of comparison, the 550 nm total aerosol optical depth retrievals for both MODIS and PARASOL are used, as this wavelength is similar to that used by OMI and CALIPSO. For the case of MODIS, the aerosol optical depth comes directly from the L2 products, while for PARASOL the aerosol optical depth comes from using the retrieved Angstrom coefficient together with the 865 nm optical depth.

[32] Further descriptions of these three instruments and their aerosol products is given by *Herman et al.* [2005], *Remer et al.* [2005], *Torres et al.* [2007], and *Ahn et al.* [2008]. MODIS, OMI and PARASOL retrievals have been extensively validated against AERONET observations, which are a network of ground based sun photometers that are calibrated and checked regularly.

[33] Some differences between the MODIS and PARASOL retrievals are expected since MODIS assumes a spherical aerosol phase function for over-water retrievals, while PARASOL accounts for non-spherical particle shapes. Consequently the MODIS algorithm may incorrectly assign too low a value to the coarse mode fraction as well as retrieve a smaller optical depth value than PARASOL, although this has been improved in the Collection 005 version compared to previous versions [*MODIS Project*, 2006]. This should only be the case for low optical depth retrievals, since for τ_{VIS} (550 nm) ≥ 2 , multiple scattering dominates, and the two instruments should retrieve the same optical depths. Since the OMI retrieval uses two channels that are only 34 nm apart, most of the phase function effects cancel, making non-sphericity a second order effect. AIRS is not very sensitive to the shape of the dust particles since their sizes are typically a few microns, much smaller than thermal infrared wavelengths.

[34] Table 2 summarizes some characteristics of the instruments mentioned in this paper. The differing swath widths affect the size of the data gaps in the tropical zones, where the swath coverage from adjacent orbits does not view some areas of the Earth's surface.

5. February 20–24, 2007, Dust Storm Over North Africa

[35] Data from daytime passes of the A-Train instruments showed a large dust storm advecting over the northern Sahara for five consecutive days in late February 2007. These

passes were all roughly within a two hour window centered around 12:00 UTC. MM/DD is used as shorthand for dates, where MM is the month and DD is the day.

[36] The geostationary day/night SEVIRI images confirm that the storm started around midday 02/20 after an Atlantic storm entered the African continent over Morocco and Western Algeria. The storm then progressed over parts of Mauritania and Mali, both known hot spots of dust emission [*Engelstaedter and Washington*, 2007], towards south central Algeria (02/21), east Algeria (02/22), north Libya (02/23), and finally over the waters of the Eastern Mediterranean (Egypt, Syria, Turkey) on 02/24. In between, dust was also seen in (midnight) night time passes of AIRS and CALIPSO. The cyclone and dust were mainly coincident during the early stages, but by 02/23 the cyclone started to dissipate, with most of the dust leading the cyclone remnants, and a smaller part advecting towards the Red Sea.

[37] This storm presents an ideal opportunity to compare A-Train dust optical depth retrievals over land, over ocean, and across land-sea boundaries. The combination of viewing geometry and overpass times and cloud cover meant that for the first 18 hours, the AIRS DDA detected dust for only a small portion of the storm. From noon 02/21 onwards, for four days and nights, AIRS was much better positioned for dust detection. Comparisons of the combined retrieved TIR optical depths from 02/21 to 02/24 against daytime visible images (from MODIS and SEVIRI) and nighttime thermal infrared images (from AIRS and SEVIRI) confirm the passage of the mid-latitude cyclone, which was roughly centered around ECMWF peak wind-speed tracks.

[38] The sands of the North African deserts of Libya, Algeria and Tunisia over which this dust storm passed contain carbonates such as calcite [*Formenti et al.*, 2008]. In addition, the soils of these areas should have less kaolinite than the soils of the southern Sahara and Sahel [see, e.g., *Claquin et al.*, 1999; *Grassian*, 2005]. Optical depths retrieved from another source of optical constants, the mineral transported (MITR) optical constants from the OPAC database [*Hess et al.*, 1998], are only $\sim 1.1 \pm 0.10$ times larger than those retrieved with our default set of optical constants from *Volz* [1973]. Optical constants for kaolinite from *Roush et al.* [1991] gave similar optical depths to OPAC and Volz ratios, but contain spectral features that are not seen in the observed spectra. An examination of the spectral residuals obtained from these different databases demonstrated that the Volz database of optical constants was the most appropriate for this dust storm. A noticeable feature around the 860–880 cm⁻¹ region was seen

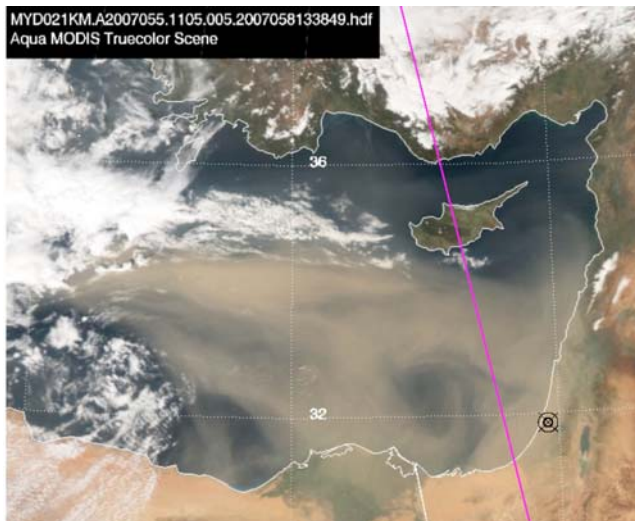


Figure 2. True color image using MODIS visible channels of 02/24/2007 dust storm in the Eastern Mediterranean, obtained at 11.05 UTC. Dust is the main contaminant over a large area of the sea. CALIPSO track is in magenta, and Nes Ziona AERONET site in black.

in the spectra, and can be attributed to carbonates expected in desert dust originating from N. and N.W. Africa.

6. Over Water Optical Depth Comparisons

[39] Figure 2 is the 02/24 MODIS visible image taken at $\approx 11:05$ UTC. Dust is clearly seen over a large, cloud-free area over the eastern Mediterranean Sea. The Nes Ziona AERONET site is shown by the crossed circle. The line in magenta shows the ground track of the CALIPSO overpass, going from the Israel/Egypt border towards Turkey. All the A-Train instruments have a significant number of dust retrievals.

[40] Along the track shown, the CALIOP 532 nm depolarization ratio was usually larger (≈ 0.25) for the lower layer, and smaller for the upper layer (≈ 0.15), implying the presence of smaller particles higher up, to which AIRS is less sensitive. The depolarization ratio (not shown here, but between 0.2 and 0.3) is slightly lower than the 0.32 ± 0.01 reported by Liu *et al.* [2008] for the case of an August 2007 dust storm tracked moving westwards across the Atlantic, but are in agreement with the CALIOP dust classification scheme. That scheme (SIBYL) uses a latitudinally dependent depolarization threshold [Young and Vaughan, 2009], but typically does not exceed 0.4 for dust [Liu *et al.*, 2008].

6.1. Retrieved Dust Heights

[41] Figure 3 shows the CALIOP backscatter data (in units of $\text{km}^{-1} \text{sr}^{-1}$) from 0–5 km (with the vertical colorbar showing this backscatter multiplied by 1000) along the CALIOP track. The black line denotes ground (or sea) level. CALIOP backscatter data less than a minimum threshold value ($0.75 \times 10^{-3} \text{ km}^{-1} \text{sr}^{-1}$) are masked out for clarity. The solid horizontal line along the top of the plot shows the peak measured backscatter above 5 km. A large backscatter here roughly indicates the presence of thick cloud above the dust, such as at 37 N.

[42] Close to Egypt (at 31 N), a thick layer of dust is present from 1–2 km, with a very tenuous layer between 3–4 km. South of Cyprus (35 N), the dust resides in a single layer between 1–2 km, which rises to 4 km close to Turkey (at 36 N).

[43] On the same plot, the blue curve shows the mean retrieved dust top heights using the AIRS FOVS matched to the CALIOP track. Averaging over the FOVs in each $0.5^\circ \times 0.5^\circ$ grid box provides a height uncertainty of $\sim \pm 0.5$ km, which is the standard deviation of the retrieved aerosol layer heights among the AIRS fields of view typically found within such regions.

[44] As shown in Figure 3, CALIOP can measure details of the vertical dust structure, unlike our AIRS height retrieval algorithm, which averages the optimal dust tops of a 3×3 Field of Regard, and reports only the averaged dust top. Figure 3 shows that the AIRS retrieved height tracks the thicker part of the dust measured by CALIOP, even when there is an overlying tenuous second layer (e.g. close to Egypt). The CALIOP depolarization data shows that this upper tenuous layer from 30 to 33 degrees latitude is more consistent with fine mode aerosols that AIRS cannot detect.

[45] Figure 4 shows the heights retrieved by AIRS, compared to the GOCART climatology used by OMI (Figure 4, right). For this case, the average climatology places the dust about 1 km too high, which will produce lower retrieved optical depths both for AIRS (TIR) and OMI (UV), as shown in the next section.

6.2. Retrieved Optical Depths Along CALIOP Track

[46] AIRS retrievals of the dust optical depths were performed using three different estimates of the dust vertical profiles. The first (case I) used a dust profile shape derived

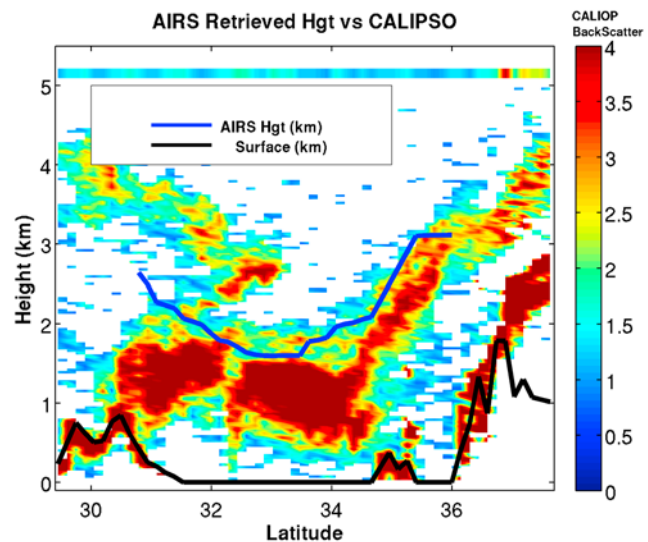


Figure 3. CALIPSO data showing dust top height for the 02/24/2007 dust storm. The attenuated backscatter is plotted, with Latitude on the horizontal axis, and height on the vertical axis. The horizontal bar at 5.25 km shows the peak backscatter for heights above 5 km. Two dust layers are clearly seen close to Egypt, and a rising layer close to Turkey. Dust top heights retrieved from the AIRS data are shown by the blue line, with a ± 0.5 km error bar.

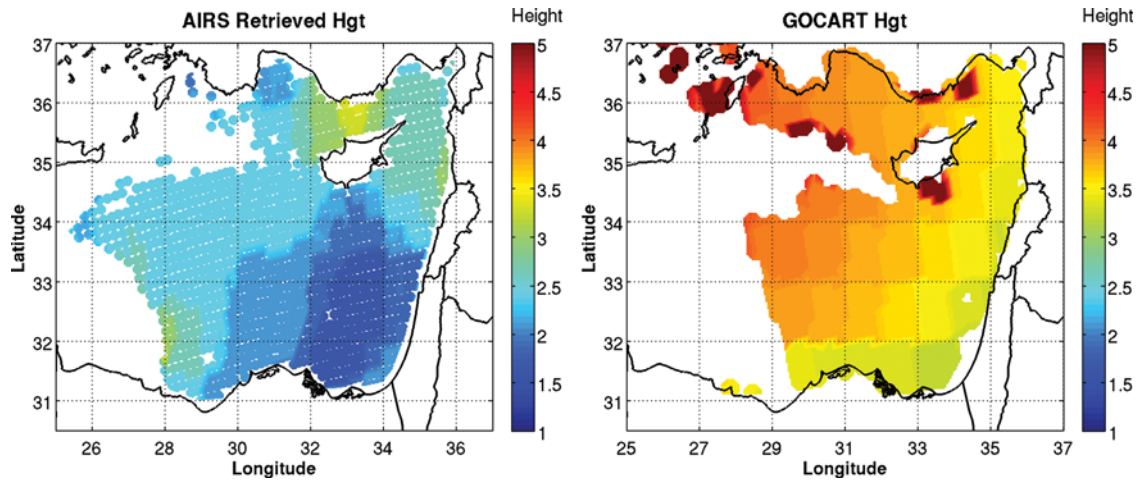


Figure 4. Dust heights in km, retrieved from (left) AIRS versus (right) GOCART climatology used by OMI. The color scales on each plot are the same. Notice that the climatology heights are higher than the AIRS retrieved heights. The AIRS retrieved heights are in good agreement with those derived from CALIOP data, as is shown in Figure 3.

from CALIOP. The second approach (case II) used the AIRS radiances themselves to estimate the height of the dust layer. Following OMI, retrievals were made using the GOCART climatological heights for dust (case III).

[47] A two-slab dust profile can be obtained directly from the CALIOP extinction data, by assuming the lidar extinction is proportional to the total mass of the dust and quantitatively estimating the vertical aerosol loading profile averaged over an AIRS footprint. Along the CALIOP track, fifty individual CALIOP profiles (spanning a total of 15 km) are averaged to estimate the dust profile for one AIRS FOV retrieval. Each average CALIOP vertical profile is further smoothed into a maximum of two distinct dust “slab” layers. This is done with a two-layer detection algorithm based on a two-peak Gaussian non-linear fit to the extinction profiles in order to obtain the mean heights, widths, and relative weighting. The overall results are independent of small variations of the relative weights of these slabs. This approach is of course only possible for AIRS FOVs collocated with the CALIPSO track. In addition, the CALIOP data may not accurately represent the dust vertical structure when very thick dust (or a cloud) prevents CALIOP from penetrating into the lower parts of the atmosphere.

[48] A second retrieval (case II) uses AIRS derived heights shown in Figure 3. Finally, a third retrieval (case III) used the GOCART climatological height, shown in Figure 4. Comparison of Figures 3 and 4 shows the climatological height is higher than the CALIOP or AIRS retrieved heights except close to the Turkish coast.

[49] Figure 5 shows the resulting optical depths of all instruments along the CALIPSO track. Values over land (latitudes less than 31 N, greater than 36 N) and a water cloud near Cyprus at (33E, 34.5N) have been masked out. The nearest AERONET site to the CALIPSO ground track was Nes Ziona, which registered a peak τ_{VIS} (500 nm) of 3.3 at 11:00 UTC (close to the Aqua overpass time), while the peak optical depth for the A-Train instruments range from 3 (AIRS $\times 4$) to about 3.7 (PARASOL). This AERONET site is located at (32N, 35E) and as seen from Figure 2 is near

Egypt where the peak A-Train optical depths were retrieved. The AIRS optical depths are scaled by a factor of four to compare to the 500 nm aerosol optical depths. This factor is consistent with work by *Highwood et al.* [2003], and arises

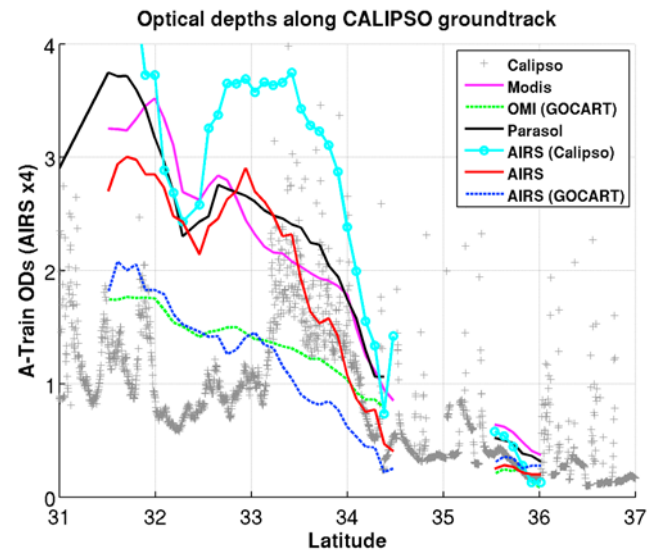


Figure 5. Optical depth as a function of Latitude along the CALIPSO track, for the different A-Train instruments on 02/24/2007. Egypt is on the left, Turkey on the right, and Cyprus is roughly centered at 35N. A factor of $\tau_{VIS}/\tau_{IR} = 4$ is used. For ease of comparison, the optical depths can be grouped into three categories. The solid curves, with MODIS in magenta, PARASOL in black and AIRS (II) in red show these three retrievals are very well correlated, and agree in magnitude. The dashed curves, with OMI in green and AIRS in blue, use GOCART climatology. Finally the CALIOP data is used for the AIRS (I) retrieval shown in cyan, and the CALIPSO optical depths shown as dark grey crosses.

Table 3. February 24, 2007, Summary of Regressions Along CALIOP Track: Regression Done Against MODIS $\tau(550\text{ nm})$

Instrument	Slope	Intercept	Correlation Coefficient R
CALIOP (532 nm)	0.22	0.58	0.46
PARASOL (550 nm)	1.00	0.20	0.95
OMI (500 nm)	0.22	0.57	0.91
AIRS I (900 cm^{-1})	0.27	0.23	0.85
AIRS II (900 cm^{-1})	0.25	-0.01	0.95
AIRS III (900 cm^{-1})	0.14	0.02	0.95

mainly due to differences in the dust composition (optical constants) and particle size distributions used in the retrieval algorithms for measurements at the VIS/UV wavelengths.

[50] The use of climatological versus retrieved heights immediately demonstrates the sensitivity to height: a higher dust height leads to a smaller retrieved TIR optical depth, and vice versa. Retrievals using one effective dust layer at the correct height yield similar results to using a weighted two layer approach from the CALIOP data. North of 35N there is a smaller spread in the three AIRS retrievals since the climatology, retrieved, and actual heights agree better. For all three cases, the spectral bias and standard deviation are close to the AIRS noise level of 0.2 K.

[51] Table 3 summarizes the optical depth correlations of all the instruments against MODIS, along the CALIOP track. Collectively, the high (Pearson) correlation coefficients ($R \geq 0.7$) show the retrievals for the suite of instruments are well correlated with MODIS. In particular, the two visible instruments, PARASOL and MODIS, agree very well. OMI has comparatively lower optical depths, as it used the GOCART height climatology which is generally higher than the CALIOP data (or AIRS retrievals).

[52] CALIOP has the lowest correlation with MODIS. The 532 nm derived CALIOP optical depths (gray crosses) agree for the lower optical depth values north of about 33.5N, but disagree at higher optical depths. For this paper,

we used our own extinction retrieval algorithm, which was compared to the Level 2 CALIPSO project extinction algorithm for this case. At higher optical depths, CALIPSO extinction deviates significantly from column optical depths, and until this is fully resolved, use of these data is premature. The discrepancies between the CALIOP retrieved optical depths and those retrieved from the passive instruments arise from the fact that the lidar retrievals assume single scattering. The CALIPSO project scientists (M. Vaughan, personal communication, 2009) do not believe that multiple scattering will be significant for this case, but multiple scatter calculations have not been carried out here. For a similar case, multiple scattering was conjectured to be present [Liu *et al.*, 2009]. The CALIPSO Algorithm Theoretical Basis Document (ATBD) shows little difference in multiple scattering for a wide range of extinction values expected from aerosol layers of less than 1 km^{-1} extinction and thickness up to 1 km. Notably, this dust layer is at the upper range of the multiple scattering calculations shown in the ATBD and is in fact thicker than that studied in the ATBD.

6.3. Retrieval Comparisons for Entire Region

[53] AIRS, MODIS, POLDER, and OMI dust retrievals for the entire dust storm (not just along the CALIOP track) are compared here. In this case, only AIRS case II and case III retrievals are possible. Only the case II retrievals are presented (AIRS derived dust height), although both the case II and III retrieved optical depths exhibit dust patterns that are very similar to those in Figure 2.

[54] Figure 6 compares the AIRS retrieved $\tau_{IR}(900\text{ cm}^{-1}) \times 4$ (Figure 6, left, using our retrieved heights) and the total MODIS $0.55\text{ }\mu\text{m}$ product (Figure 6, right). The crosses show the CALIPSO track. AIRS produces retrievals over a larger area than MODIS, which has no data in the region north of Egypt between 26–30 E due to sun glint.

[55] For this over-ocean data set, the AIRS optical depths were retrieved using the effective radii of the total size distribution derived from PARASOL, which is close to $2\text{ }\mu\text{m}$

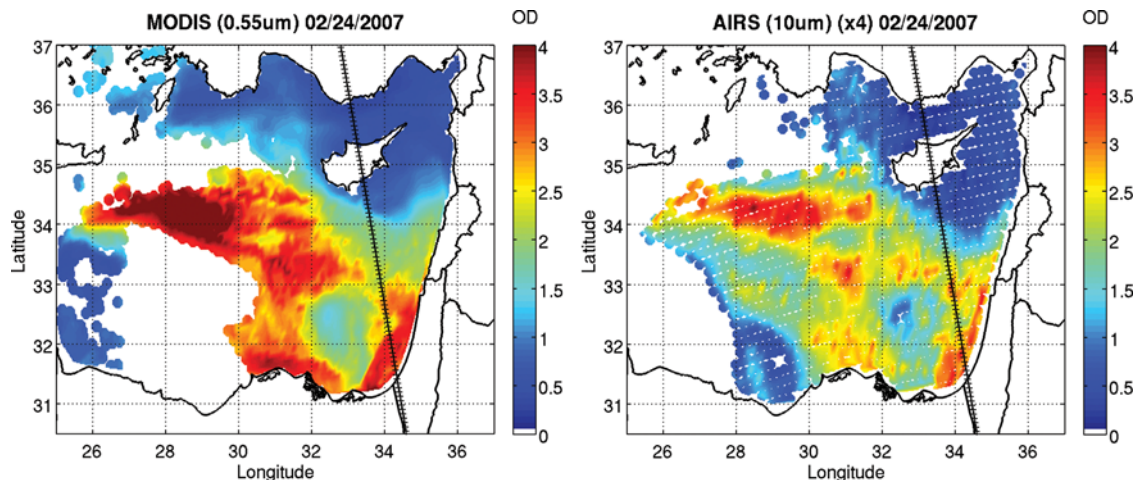


Figure 6. (left) MODIS Aerosol $\tau_{MODIS}(550\text{ nm})$ product compared with (right) thermal IR AIRS $\tau_{IR} \times 4$, using dust heights from the AIRS retrievals. The blank region in the MODIS plot is an area of sun glint contamination.

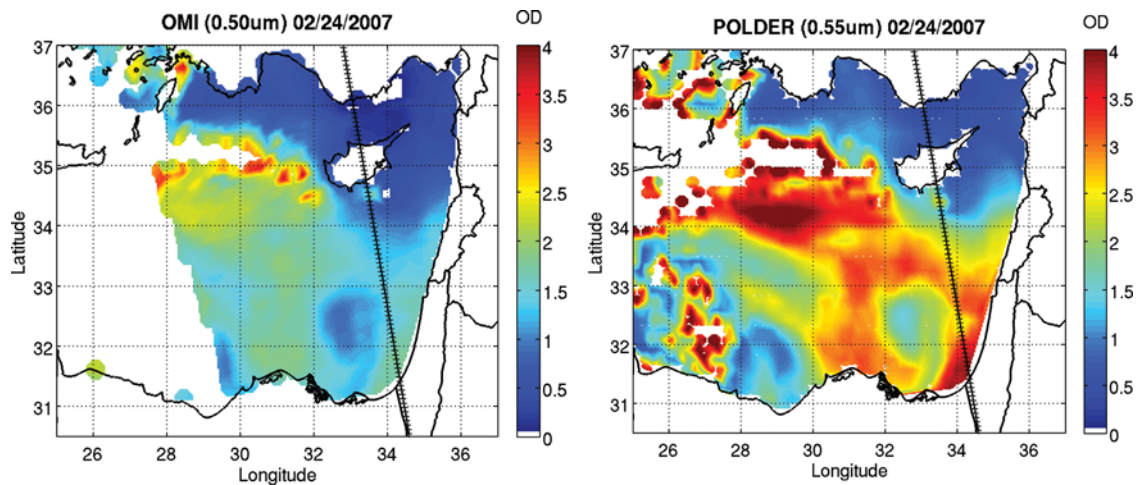


Figure 7. (left) OMI and (right) PARASOL optical depths. OMI is affected by sun glint in the region west of 30E. PARASOL has cloud screening turned off.

everywhere except northeast of Cyprus, where it drops to about $\simeq 1.5 \mu\text{m}$. This slightly lower value for the radii lowers the optical depths by a factor of 0.8 over that obtained using the default $2 \mu\text{m}$ value, leading to an incremental improvement of the overall MODIS versus AIRS correlation.

[56] Figure 7 shows the OMI $0.50 \mu\text{m}$ retrieved optical depths (Figure 7, left) and the $0.55 \mu\text{m}$ PARASOL retrieval (Figure 7, right). The OMI retrievals are limited to those pixels where cloud was undetected in the FOV. The GOCART climatology used in the OMAERUV retrieval for this dust storm yields optical depths that are smaller compared to the other instruments. A comparison to Figure 6 suggests that OMI is also affected by sun glint. The multi-angle capability of PARASOL (up to 16 view angles) provides a few scene geometries that are outside the glint, although the derived aerosol model and optical depth are not as accurate due to the reduced angle coverage.

[57] Starting with the OMI FOVs, linearly weighted averages of the AIRS, MODIS and PARASOL retrievals were made, weighted by the distance away from the center of the OMI footprint. Figure 8 compares these results. MODIS $0.55 \mu\text{m}$ total optical depths are on the horizontal scale, while the vertical scale shows the column optical depths from the other instruments (with the TIR optical depths multiplied by 4).

[58] Figure 8 shows that AIRS retrieved optical depths using GOCART climatology (blue) are much smaller than AIRS retrieved optical depths derived directly from the AIRS radiances (red), since the climatological heights are higher than the derived heights. For this set of retrievals, the AIRS optical depths using the retrieved heights (red curve) agree very well with the PARASOL retrievals (black curve).

[59] The best quality OMI data (minimum cloud contamination detected) is in the region between 30E to 36 E, from about 35 N to the southern coast of Turkey. Here, the GOCART climatological dust height agrees with CALIPSO and the AIRS retrieved heights, with $\tau_{\text{OMI}} = 1.205\tau_{\text{MODIS}} - 0.073$, with a correlation $R \simeq 0.927$. Lowering the OMI quality criteria to allow for cloud contamination yields much

greater area coverage, to areas south of 35 N towards the Egyptian coast. However, as described earlier, GOCART heights for this extended region are higher than those derived from AIRS, with $\tau_{\text{OMI}} = 0.408\tau_{\text{MODIS}} + 0.812$, $R \simeq 0.832$. The smaller OMI optical depths again suggest the GOCART heights may be too high. After including both the best and good quality FOVS (as shown in Figure 7), we obtain a final $\tau_{\text{OMI}} = 0.502\tau_{\text{MODIS}} + 0.544$, $R \simeq 0.905$.

[60] The PARASOL optical depths, reported at 865 nm, are similar to values obtained at 550 nm since the Angstrom Coefficient $\alpha(\text{PARASOL})$ is close to zero for dust. This

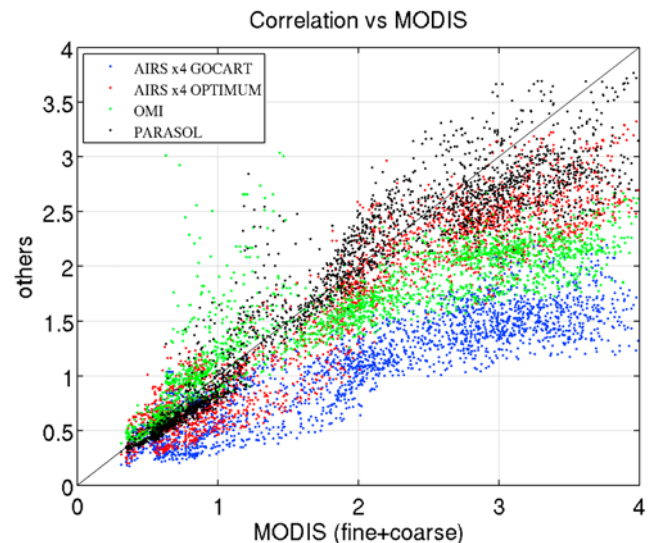


Figure 8. Comparison of optical depths over the Mediterranean, for the A-Train suite. MODIS 550 nm total optical depths are plotted on the horizontal axis. Two AIRS comparisons (multiplied by 4) are shown, one using GOCART climatology (blue) and one using the retrieved heights (red). PARASOL (black dots) and OMI (green dots) comparisons are also shown.

Table 4. February 21–24, 2007, Summary of Regressions Against MODIS 0.55 μm Optical Depth for All Instruments^a

Date in Feb 2007	AIRS (900 cm^{-1}) (Corr) Slope, Int	OMI (0.50 μm) (Corr) Slope, Int	PARASOL (0.55 μm) (Corr) Slope, Int
21 (L)	(0.537) 0.127 MOD + 0.091	(0.579) 0.913 MOD + 0.484	(N/A) N/A MOD + N/A
22 (L)	(0.664) 0.129 MOD + 0.077	(0.765) 0.847 MOD + 0.635	(N/A) N/A MOD + N/A
23 (L)	(0.252) 0.047 MOD + 0.240	(0.268) 0.222 MOD + 1.693	(N/A) N/A MOD + N/A
23 (W)	(0.779) 0.153 MOD + 0.232	(0.541) 0.257 MOD + 1.199	(0.749) 0.646 MOD + 1.392
24 (W)	(0.938) 0.182 MOD + 0.036	(0.854) 0.460 MOD + 0.340	(0.946) 0.830 MOD + 0.383

^aL denotes land; W denotes water; MOD refers to the 0.55 μm MODIS optical depth.

coefficient measures how the optical depth varies with wavelength λ : $\tau(\lambda) = \tau_{\lambda_0} \times (\lambda/\lambda_0)^{-\alpha}$. A small α value means the scattering is dominated by coarse material in the aerosol, while a large exponent implies the aerosol is dominated by fine mode particles. The larger values observed at (31.5E, 35.5N) and west of that location are due to cloud contamination. The PARASOL versus MODIS retrievals are roughly equal for $\tau_{\text{MODIS}} \leq 2$, while for larger values, the PARASOL retrievals are slightly smaller than MODIS.

[61] The PARASOL dust model has no absorption and no spectral dependence. The PARASOL algorithm also assumes non-spherical particles, and should be able to reliably retrieve the asymmetry factor, effective radius and fine mode fractions. However, the algorithm may switch to large spherical models for high optical depths when absorption starts to be important, and this may explain the dispersion in the retrievals. The optical thickness retrieved by PARASOL over the area near the Egypt/Israel coast is about 3.1–3.3 at 550 nm. This value is consistent with the AERONET retrievals from Nes Ziona, which are around 3.3 at the satellite overpass time.

[62] The retrieved PARASOL dust effective radii for this data set had two peaks. The region between the N. African shore and Cyprus consisted of particles whose retrieved effective radius was $2.0 \pm 0.25 \mu\text{m}$, with $\alpha(\text{PARASOL}) \simeq 0.2 \pm 0.1$. Between 35 N (Cyprus) and the Turkish coast, the retrieved PARASOL dust effective radius and Angstrom coefficient ($\alpha(\text{PARASOL})$) was about $1.5 \pm 0.5 \mu\text{m}$, $\simeq 0.6$. The retrieved dust loading for this region is much less than for the first region. For the entire region, PARASOL retrieved an asymmetry factor of about 0.775 ± 0.025 . Conversely for the region between Cyprus and the N.African coast, $\alpha(\text{MODIS})$ was bimodal, with one peak at 0.2 ± 0.05 and another peak at 0.45 ± 0.075 . South of Cyprus the ratio of PARASOL 865 nm coarse mode to total (coarse + fine) optical depth is $\simeq 0.95$, while north of Cyprus the ratio drops to ≤ 0.25 .

[63] Compared to PARASOL, MODIS shows a much larger fine mode contribution. For the 865 nm MODIS channel the coarse mode fractions were about 0.8 and 0.6 for the dust areas south and north of Cyprus. As noted above, the MODIS retrieval algorithm could over-estimate the fine mode contribution, as it assumes the aerosol consists of spherical particles. In addition, the effective radius retrieved by MODIS is about $0.75 \mu\text{m}$ south and south west of Cyprus and $0.50 \mu\text{m}$ north east of Cyprus. The asymmetry factor retrieved by MODIS was slightly smaller than that retrieved by PARASOL, namely 0.65–0.70.

[64] Table 4 includes a summary of dust retrievals. As mentioned previously, the PARASOL $\tau(865 \text{ nm})$ is converted to 550 nm using the retrieved Angstrom coefficient. Figures 6 and 7 and Table 3 demonstrate that all instruments see roughly the same features. AIRS optical depth retrievals are dependent on height information, which were simultaneously retrieved in this paper. OMI optical depth retrievals are also dependent on height, and currently use GOCART climatology. Since Figures 6 and 7 show differing areal coverage by the instruments, Table 5 lists the correlations when the instruments are paired and regressed against each other, meaning the areal coverage would be different for different pairs in the table. Note that a few very high AIRS optical depths ($\tau_{\text{IR}} \geq 4$) have been rejected in the comparison, since AIRS cannot reliably retrieve high optical depths. AIRS and OMI are reported at 900 cm^{-1} and 500 cm^{-1} , while MODIS and PARASOL are both reported at 550 nm.

7. Summary of Results for Other Days

[65] Daytime observations earlier in the storm were mainly over land. AIRS dust height retrievals over land sometimes returned values close to or below 1 km, because of low thermal contrast and possibly inaccurate surface emissivities. Large optical depths were also retrieved for such FOVS. In these instances, the minimum dust top in the retrieval was set to a height of 1 km.

[66] The CALIOP track was sufficiently close to AIRS to be useful for validating the AIRS height retrievals for data obtained after 13.30 UTC on 02/21. Along the CALIOP track, the retrieved AIRS heights compare favorably, both over ocean and land. For example over land on 02/23–02/24, the correlation coefficient between the retrieved AIRS height versus the CALIOP heights was 0.65, with the lower correlations occurring when CALIOP indicated low dust over land, or when the height changed rapidly (e.g. when going from land to ocean). Some FOVs had both a dust signature ($\text{BT}960 \leq \text{BT}820$) and low BT820 values, which indicates thin high cloud over the dust. PARASOL coarse mode retrievals are only available for the over-ocean part of the dust storm on 02/23 and 02/24. For the other days, the dust was mainly over land for which only fine mode retrievals are available.

[67] Table 4 summarizes the intercomparison of retrieved optical depths for daytime coincident views of dust by AIRS, OMI and MODIS (and POLDER coarse mode retrievals, when available over ocean only). The “L” and “W” indicates retrievals over land or water, and regressions for the different instruments are made versus MODIS, with the correlations

Table 5. February 24, 2007, Summary of Regressions Among Pairs of Passive Instruments

Instrument y	Instrument x	Correlation Coefficient R	Slope	Intercept
AIRS	MODIS	0.92	0.19	0.04
OMI	MODIS	0.86	0.47	0.32
PARASOL	MODIS	0.82	0.72	0.76
AIRS	PARASOL	0.91	0.20	0.00
OMI	PARASOL	0.88	0.54	0.19
OMI	AIRS	0.80	2.24	0.39

in parentheses. The correlations between the instruments are noticeably lower over land than over water, as illustrated below.

[68] Figure 9 is a daytime ($\approx 12:00$ UTC) Aqua-MODIS true color image for 02/23, showing dust blowing over the Great Sand Sea (Libya) into the Gulf of Sindh and over the Mediterranean. The retrieved PARASOL dust effective radius for this data set had a broad peak in the $2.0\text{--}2.5\text{ }\mu\text{m}$ region, and was used for the over-ocean AIRS retrievals. The CALIOP data showed a 1.25 km thick dust layer, with average height about 1.5 km inland until 29°N , that rose slowly to about 3.5 km over the sea around 35°N . Figure 10 compares the AIRS retrievals (Figure 10, left) with MODIS retrievals (Figure 10, right). The AIRS optical depths are seen to have a smooth transition from land to ocean. This could be very important for A-Train dust characterization, since MODIS retrievals can exhibit physical discontinuities (such as in this data set).

[69] PARASOL (865 nm) retrieved slightly larger optical depths than MODIS (550 nm), with a lower correlation coefficient than for 02/24. For optical depths less than 1.5, the PARASOL (865 nm)/MODIS (550 nm) ratio was close to unity. Taking into account all retrieved optical depths, Table 4 shows a non-unity slope and non-zero intercept. This is attributed to a significant tail in the distribution for optical depth ratios ≥ 1.5 . The retrieved Angstrom coefficients are again similar for MODIS and PARASOL, though for $\tau_{VIS} \leq 2$, $\alpha(\text{MODIS})$ is about double the $\alpha(\text{PARASOL})$ value of $\approx 0.25 \pm 0.1$ value; for $\tau_{VIS} \geq 2$, the α values were roughly similar (≤ 0.2).

[70] The GOCART climatology for the OMI retrievals again gave values typically 1 km higher than those retrieved by AIRS. This again made OMI optical depth retrievals comparatively smaller than those from the other instruments. Over ocean, the OMI (500 nm)/MODIS (550 nm) optical depth ratio was 0.8 ± 0.2 . Typically the OMI retrievals were proportional to MODIS retrievals for $\tau_{VIS} \leq 2$, but then flattened out for larger optical depth values. Conversely over land, the OMI/MODIS optical depth ratio was about 1.5 ± 0.5 , implying many OMI retrievals had values larger than the MODIS Deep Blue results.

[71] The AIRS (900 cm^{-1})/MODIS (550 nm) optical depth ratio over ocean (using our retrieved heights) was 0.25 ± 0.1 , similar to 02/24. This optical depth ratio changed to about 0.4 over land. Over ocean, the correlations between the MODIS and AIRS optical depths are slightly lower than for 02/24 (≥ 0.8). However, over land the correlations

between the MODIS and AIRS retrievals are noticeably smaller. This could be due to errors in the retrievals by either instrument, and certainly more work is needed for the AIRS retrieval over land.

8. Direct Estimate of OLR Forcing

[72] Outgoing longwave radiative (OLR) forcing by dust has received very little attention in the literature. Although longwave dust forcing is smaller than shortwave forcing, it still remains a highly uncertain quantity. Day time long wave radiative forcing by dust is much larger over land than over ocean, as there is a significant temperature gradient between land and the atmosphere [Haywood *et al.*, 2005]. Dust OLR forcing is concentrated in the $10\text{ }\mu\text{m}$ window region, where the only significant absorbers are water vapor and ozone, which are reasonably well characterized, for the purposes of OLR, within the ECMWF forecast model.

[73] The OLR dust forcing can be estimated directly from the AIRS TIR data without a simultaneous dust optical depth/height retrieval, if one can compute the OLR if no dust were present, which can be done using the ECMWF model data. We have previously shown that ECMWF model data, for clear fields of view, can reproduce the AIRS radiances very accurately using our radiative transfer model [Strow *et al.*, 2006].

[74] Let r^i denote the AIRS radiance of channel i , and $r^{i,\text{clearcalc}}$ denote a clear sky radiance estimate. The OLR forcing is then approximately $f(\theta)\gamma\sum_i(r^{i,\text{clearcalc}} - r^i_d)\pi$, where γ (≈ 0.85) is an empirical factor derived from comparisons to flux computations using line-by-line calculations, and accounts for the finite widths and spectral gaps of the AIRS channels, and $f(\theta)$ is an angular correction. This estimate is quite insensitive to detailed knowledge of dust

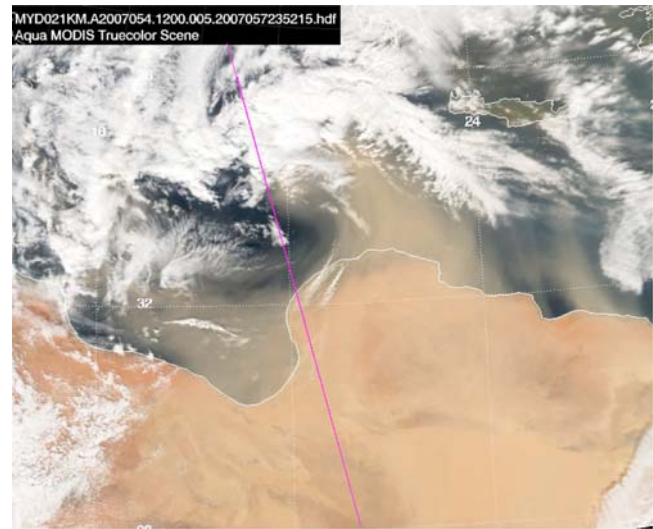


Figure 9. True color image using MODIS visible channels of 02/23/2007 dust storm in the Eastern Mediterranean, obtained at 12.00 UTC. Dust is seen mainly over the Libyan Desert, with only some dust visible over the sea. CALIPSO track is in magenta.

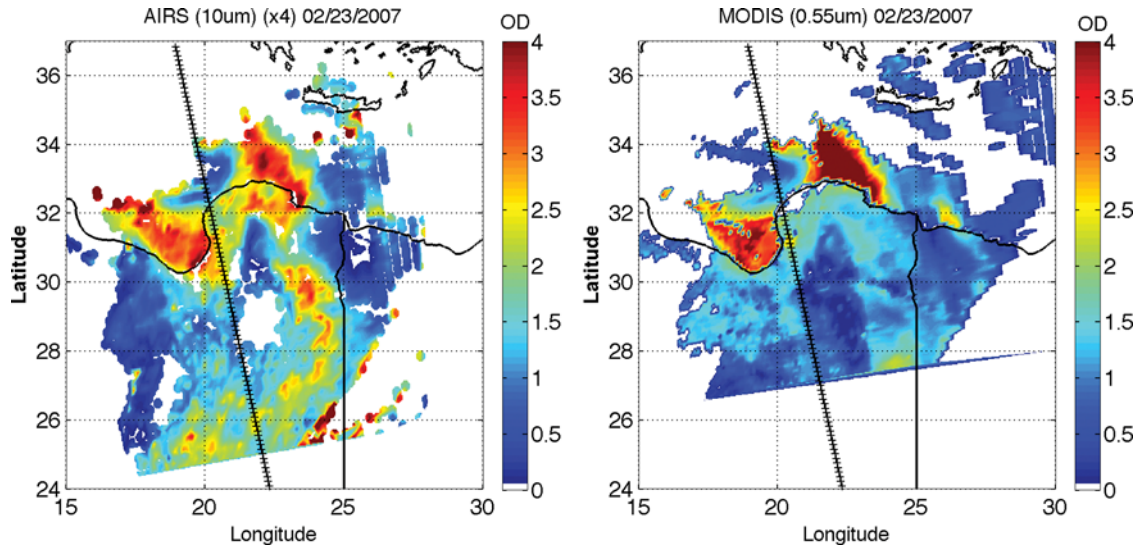


Figure 10. (left) AIRS dust on 02/23/2007 compared to (right) MODIS. CALIPSO ground tracks are shown as crosses. The images show the region for which optical depths were retrieved. Some of the retrieved AIRS optical depths over land, such as those near (27E, 27N) did not meet the post-processing quality checks and are discarded in the correlation comparisons shown in Table 4.

optical properties, though it requires an accurate atmospheric profile for $r_{clearcalc}^i$.

[75] Comparisons of our estimates of clear sky upwelling flux at the top of the atmosphere (TOA) with those reported in the AIRS Level2 OLR product, show agreement within $\pm 1 \text{ W/m}^2$. This simple approach works well since the AIRS observations, and the dust forcing, are near the peak of Planck function for terrestrial temperatures.

[76] The average OLR forcing for the 02/24/2007 storm over the Mediterranean was $\simeq +6.0 \text{ W/m}^2$ per unit infrared optical depth (or $+1.5 \text{ W/m}^2$ per unit visible optical depth), where the positive sign implies the absorbing dust reduces the OLR. The north eastern regions of the Mediterranean had higher values of forcing per unit optical depth, since the higher altitude dust absorbs and re-emits radiation at lower temperatures than the surface. A short wave forcing estimate for the entire region, using precomputed lookup tables [Remer and Kaufmann, 2006] with the MODIS retrievals was $-50 \pm 5 \text{ W/m}^2$ per unit visible optical depth.

[77] Over land, the atmospheric dust is much cooler than the surface temperature, significantly reducing the OLR. Separating the OLR components for the 02/23/2007 dust storm into sea and land, the OLR forcing is estimated to be $\simeq +10$ and $+17.5 \text{ W/m}^2$ per unit infrared optical depth respectively. These numbers are consistent with those reported in the literature from other dust storms [Highwood *et al.*, 2003].

9. Conclusions

[78] Optical depths and dust heights retrieved by TIR instruments have been shown to compare favorably against those obtained from VIS or UV instruments, with $\tau_{IR} \simeq \tau_{VIS}/4$. An advantage of TIR instruments is the ability to perform retrievals at night.

[79] The retrieved AIRS heights compare well against data from an active lidar (CALIOP). Optical depth comparisons have been made against a suite of UV/VIS A-Train instruments, showing that over ocean there is good agreement between AIRS, PARASOL, MODIS and OMI, although AIRS is the least sensitive to low optical depths. The spatial coverage of these instruments can be quite different since AIRS can retrieve dust at night and is insensitive to sun glint during the day. Over land the agreement among instruments is less satisfying. MODIS, for example, appears to exhibit unphysical gradients in dust optical depths along coastal boundaries. However, AIRS dust retrievals over land require accurate surface emissivities, and will require further work to validate in any detail.

[80] A rapid estimation of OLR forcing by TIR instruments was also presented. This estimate requires accurate surface temperatures, which are retrieved simultaneously with the dust loading.

[81] The CALIOP retrieval scheme needs further validation for optical depths ≥ 2.0 , as it currently only uses single scattering. AIRS, MODIS, and PARASOL total extinctions agree over the ocean; however MODIS may overestimate the fine mode contribution since it assumes spherical particles. As with AIRS, dust optical depth retrievals from OMI are strongly dependent on the height of the dust layer used, although we have shown that dust layer heights can be retrieved from the AIRS radiances.

[82] **Acknowledgments.** We acknowledge the use of ECMWF model fields to compute radiances. We thank Brent Holben, Emilio Cuevas and Arnon Karnieli and their staff for establishing and maintaining the AERONET sites used for this work. We acknowledge Mark Vaughan for many helpful discussions, and Dave Turner and Ted Roush for readily providing optical constants for various dust species. PARASOL satellite data were processed by ICARE data center (<http://www-icare.univ-lille1.fr/icare/main.php>).

Lorraine Remer and Shana Mattoo provided the MODIS SW forcing estimates. We also thank L. Gonzalez and C. Deroo for the SEVIRI data processing. We also gratefully acknowledge the numerous helpful comments and suggestions made by the anonymous referees. This work was supported by NASA grant NNX08AD34G and by contract NAS1-99107 for Calipso Science Team support to the NASA Langley Research Center. The hardware used in the computational studies is part of the UMBC High Performance Computing Facility (HPCF). The facility is supported by the U.S. National Science Foundation through the MRI program (grant CNS-0821258) and the SCREMS program (grant DMS-0821311), with additional substantial support from the University of Maryland Baltimore County (UMBC). See www.umbc.edu/hpcf for more information on HPCF and the projects using its resources.

References

- Ahn, C., O. Torres, and P. Bhartia (2008), Comparison of OMI UV aerosol products with Aqua-MODIS and MISR products in 2006, *J. Geophys. Res.*, **113**, D16S27, doi:10.1029/2007JD008832.
- Barnes, W., T. S. Pagano, and V. V. Salomonson (1998), Prelaunch characteristics of MODIS on EOS-AM1, *IEEE Trans. Geosci. Remote Sens.*, **36**, 1088–1100.
- Borbas, E., L. Moy, S. Seeman, R. Knuteson, I. Trigo, P. Antonelli, J. Li, and H. L. Huang (2007), A global infrared land emissivity database and its validation, paper presented at 11th Symposium on Integrated Observing and Assimilation Systems for Atmosphere, Oceans and Land Surfaces, Am. Meteorol. Soc., San Antonio, Tex.
- Chou, M.-D., K.-T. Lee, S.-C. Tsay, and Q. Fu (1999), Parameterization for cloud longwave scattering for use in atmospheric models, *J. Clim.*, **12**, 159–169.
- Claquin, T., M. Schulz, and Y. Balkanski (1999), Modeling the mineralogy of atmospheric dust sources, *J. Geophys. Res.*, **104**, 22,243–22,256.
- De Souza-Machado, S., L. L. Strow, H. Motteler, and S. Hannon (2006), Infrared dust spectral signatures from AIRS, *Geophys. Res. Lett.*, **33**, L03801, doi:10.1029/2005GL024364.
- Deuze, J., et al. (2001), Remote sensing of aerosols over land surfaces from POLDER/ADEOS-I polarized measurements, *J. Geophys. Res.*, **106**, 4913–4926.
- Engelstaedter, S., and R. Washington (2007), Atmospheric controls on the annual cycle of North African dust, *J. Geophys. Res.*, **112**, D03103, doi:10.1029/2006JD007195.
- Formenti, P., et al. (2008), Regional variability of the composition of mineral dust from West Africa: Results of the AMMA SOPO/ABEX and DODO field campaigns, *J. Geophys. Res.*, **113**, D00C13, doi:10.1029/2008JD009903.
- Ganguly, D., P. Ginoux, V. Ramaswamy, D. Winker, B. Holben, and S. Tripathi (2009), Retrieving the composition and concentration of aerosols over the Indo-Gangetic plain using CALIOP and AERONET data, *Geophys. Res. Lett.*, **36**, L13806, doi:10.1029/2009GL038315.
- Ginoux, P., M. Chin, I. Tegen, J. Prospero, B. Holben, O. Dubovik, and S.-J. Lin (2001), Sources and global distributions of dust aerosols simulated with the GOCART model, *J. Geophys. Res.*, **106**, 20,255–20,273.
- Grassian, V. (2005), Environmental catalysis in the Earth's atmosphere: Heterogeneous reactions on mineral dust aerosol, in *Environmental Catalysis*, p. 131, CRC Press, Boca Raton, Fla.
- Gu, Y., W. Rose, and G. Bluth (2003), Retrieval of mass and size of particles in sandstorms using two MODIS IR bands: A case study of the April 7, 2001 sandstorm in China, *Geophys. Res. Lett.*, **30**(15), 1805, doi:10.1029/2003GL017405.
- Hansell, R., K.-N. Liou, S. Ou, S. C. Tsay, Q. Ji, and J. Reid (2008), Remote sensing of mineral dust aerosol using AERI during the UAE²: A modeling and sensitivity study, *J. Geophys. Res.*, **113**, D18202, doi:10.1029/2008JD010246.
- Haywood, J., R. Allan, I. Culverwell, T. Slingo, S. Milton, J. Edwards, and N. Clerbaux (2005), Can desert dust explain the outgoing OLR anomaly over the Sahara during July 2003?, *J. Geophys. Res.*, **110**, D05105, doi:10.1029/2004JD005232.
- Herman, M., J. Deuze, A. Marchand, B. Roger, and P. Lallart (2005), Aerosol remote sensing from POLDER/ADEOS over the ocean: Improved retrieval using nonspherical particle model, *J. Geophys. Res.*, **110**, D10S02, doi:10.1029/2004JD004798.
- Hess, M., P. Koepke, and I. Schult (1998), Optical properties of aerosols and clouds: The software package OPAC, *Bull. Am. Meteorol. Soc.*, **79**, 831–844.
- Highwood, E., J. Haywood, M. Silverstone, S. Newman, and J. Taylor (2003), Radiative properties and direct effect of Saharan dust measured by the C-130 aircraft during SHADE: 2. Terrestrial spectrum, *J. Geophys. Res.*, **108**(D18), 8578, doi:10.1029/2002JD002552.
- Holben, B., et al. (1998), AERONET—A federated instrument network and data archive for aerosol characterization, *Remote Sens. Environ.*, **66**, 1–16.
- Hsu, N., S.-C. Tsay, M. King, and J. Herman (2004), Aerosol properties over bright reflecting source regions, *IEEE Geosci. Remote Sens.*, **42**, 557–569.
- Intergovernmental Panel on Climate Change (IPCC) (2007), *Climate Change 2007—The Fourth Assessment Report of the IPCC*, edited by S. Solomon et al., Cambridge Univ. Press, Cambridge, U. K.
- Jickells, T., et al. (2005), Global iron connections between desert dust, ocean biogeochemistry and climate, *Science*, **308**, 67–71.
- Joseph, J., O. Yaron, E. Yaroslavich, P. Israelvich, I. Koren, Y. Yair, A. Devir, and P. Kischka (2008), Determination of most probable height of desert dust aerosol layer from space, *J. Geophys. Res.*, **113**, D20S93, doi:10.1029/2007JD009646.
- Kaufman, Y. J., I. Koren, L. Remer, D. Tanre, P. Ginoux, and S. Fan (2005), Dust transport and deposition observed from Terra-MODIS spacecraft over the Atlantic Ocean, *J. Geophys. Res.*, **110**, D10S12, doi:10.1029/2003JD004436.
- Koren, I., Y. Kaufman, R. Washington, M. Todd, Y. Rudich, J. Martins, and D. Rosenfeld (2006), The Bodele depression: A single spot in the Sahara that provides most of the mineral dust to the Amazon Forest, *Environ. Res. Lett.*, **1**, 014005, doi:10.1088/1748-9326/1/014005.
- Liu, Z., et al. (2008), CALIPSO lidar observations of optical properties of Saharan dust: A case study of long-range transport, *J. Geophys. Res.*, **113**, D07207, doi:10.1029/2007JD008878.
- Liu, Z., et al. (2009), The CALIPSO lidar cloud and aerosol discrimination: Version 2 algorithm and initial assessment of performance, *J. Atmos. Oceanic Technol.*, **26**, 1198–1213.
- Lubin, D., S. Satheesh, G. McFarquar, and A. Heymsfield (2002), Long-wave radiative forcing of Indian Ocean tropospheric aerosol, *J. Geophys. Res.*, **107**(D19), 8004, doi:10.1029/2001JD001183.
- Masuda, K., T. Takashima, and Y. Takayama (1988), Emissivity of pure and sea waters for the model sea surface in the infrared window regions, *Remote Sens. Environ.*, **24**, 313–329.
- MODIS Project (2006), Algorithm for remote sensing of tropospheric aerosol from MODIS, technical report, NASA Goddard Space Flight Cent., Greenbelt, Md. (Available at http://modis.gsfc.nasa.gov/data/atbd/atmos_atbd.php)
- Omar, A., D. Winker, J.-G. Won, M. Vaughan, C. Hostetler, and J. Reagan (2003), Selection algorithm for the CALIPSO lidar aerosol extinction-to-backscatter ratio, paper presented at Geoscience and Remote Sensing Symposium, IEEE, New York.
- Pierangelo, C., A. Chedin, S. Heilliette, N. Jacquinet-Husson, and R. Armante (2004), Dust altitude and infrared optical depth from AIRS, *Atmos. Chem. Phys.*, **4**, 1813–1822.
- Pierangelo, C., M. Mishchenko, Y. Balkanski, and A. Chédin (2005), Retrieving the effective radius of Sahara dust coarse mode from AIRS, *Geophys. Res. Lett.*, **32**, L20813, doi:10.1029/2005GL023425.
- Reale, T., and E. Dutton (2007), A candidate GCOS atmospheric reference observations network consisting of ARM, BSRN and WMO reporting sites and satellite/in-situ data collection strategies, paper presented at 2007 Annual Meeting, Am. Meteorol. Soc., San Antonio, Tex.
- Remer, L., and Y. Kaufmann (2006), Aerosol direct radiative effect at the top of the atmosphere over cloud free ocean derived from four years of MODIS data, *Atmos. Chem. Phys.*, **6**, 237–253.
- Remer, L., et al. (2005), The MODIS aerosol algorithm, products and validation, *J. Atmos. Sci.*, **62**, 947–973.
- Roush, T., J. Pollack, and J. Orenberg (1991), Derivation of midinfrared (5–25 μ m) optical constants of some silicates and palagonite, *Icarus*, **94**, 191–208.
- Shell, K. M., and R. C. J. Somerville (2007), Sensitivity of climate forcing and response to dust optical properties in an idealized model, *J. Geophys. Res.*, **112**, D03206, doi:10.1029/2006JD007198.
- Sokolik, I. (2002), The spectral radiative signature of wind blown mineral dust: Implications for remote sensing in the thermal IR region, *Geophys. Res. Lett.*, **29**(24), 2154, doi:10.1029/2002GL015910.
- Strow, L. L., S. E. Hannon, S. DeSouza-Machado, H. E. Motteler, and D. C. Tobin (2006), Validation of the Atmospheric Infrared Sounder radiative transfer algorithm, *J. Geophys. Res.*, **112**, D09S06, doi:10.1029/2005JD006146.
- Torres, O., A. Tanskanen, B. Veihelmann, C. Ahn, R. Braak, P. Bhartia, P. Veeckind, and P. Levelt (2007), Aerosols and surface UV products from Ozone Monitoring Instrument observations: An overview, *J. Geophys. Res.*, **112**, D24S47, doi:10.1029/2007JD008809.
- Volz, F. (1973), Infrared optical constants of ammonium sulphate, Sahara dust, volcanic pumice and flash, *Appl. Opt.*, **12**, 564–568.
- Winker, D. M., W. Hunt, and C. Hostetler (2004), Status and performance of the CALIOP lidar, in *Proc. SPIE Int. Soc. Opt. Eng.*, **5575**, 8–15.
- Young, S. A., and M. Vaughan (2009), The retrieval of profiles of particulate extinction from CALIOP data: Algorithm description, *J. Atmos. Oceanic Technol.*, **26**, 1105–1119.

Yu, H., et al. (2006), A review of measurement based assessments of the aerosol direct radiative effect and forcing, *Atmos. Chem. Phys.*, 6, 613–656.

S. G. DeSouza-Machado, S. Hannon, R. M. Hoff, B. Imbiriba, J. V. Martins, K. McCann, and L. L. Strow, Joint Center for Earth Systems Technology, University of Maryland Baltimore County, Baltimore, MD 21250, USA. (sergio@umbc.edu; hannon@umbc.edu; hoff@umbc.edu;

imbiriba@umbc.edu; martins@umbc.edu; kevin.mccann@umbc.edu; strow@umbc.edu)

J. L. Deuzé, F. Ducos, and D. Tanré, Atmospheric Laboratory of Optics, University of Sciences and Technologies of Lille, F-59655 Villeneuve d'Ascq CEDEX, France. (deuze@loa.univ-lille1.fr; ducos@loa.univ-lille1.fr; didier.tanre@univ-lille1.fr)

O. Torres, Department of Atmospheric and Planetary Sciences, Hampton University, Hampton, VA 23668, USA. (omar.torres@hampton.edu)